Reducing the uncertainty in a switched amplifier-driven positioning system to the sub-nanometer level

Daniel Pechgraber, Ernst Csencsics and Georg Schitter

***Abstract*— This paper presents a comprehensive position uncertainty analysis in a switched current amplifier-driven precision positioning system with an integrated full-state control structure. A mathematical system model is used combining the mechanical, electrical, and magnetical subsystem and their dynamic couplings. Further an internal quantization error feedback in the state-observer of the control is proposed, that reduces the unwanted effect of PWM-quantization on the positioning uncertainty of the system. The presented error budgeting analysis and practical experiments on a built prototype system demonstrate fast reference position tracking and a steady-state positioning uncertainty of 0.6nm (rms), which is an improvement by a factor of 65 as compared to conventional control implementations.**

I. Introduction

High-precision positioning systems play a critical role in various high-tech applications, ranging from semiconductor manufacturing [1], atomic-force microscopy [2] to 3D-printing [3]. These systems often rely on electromagnetic Lorentz-force actuation, with its favorable properties such as a linear force-current relation and quasi-zero stiffness, which make it well-suited for precision positioning applications on the nano-scale [4].

In Lorentz-force actuated positioning systems, the prevailing control architecture involves cascaded structures with inner current and outer position control loops [5]. For driving the current in the actuator coil, switched current amplifiers are preferred over linear amplifiers for their energy efficiency and reduced heat generation [5], which is especially important in space constraint environments. However they are still often avoided due to concerns related to their voltage ripple and for electro-magnetic interference (EMI) reasons [6]. Additionally they are more challenging to implement than their linear counterpart, because more complex modulation schemes and an advanced current sensing technology is required. Especially, as the current measurement noise emerges as a significant source of positioning uncertainty, when closing the inner current-control loop [7].

For this reason major emphasis was taken on the development of high-precise switched current amplifiers and their control, e.g. by combining a Luenberger estimator and a Linear Quadratic Regulator (LQR) for fast transient response and an outer frequency domain controller [8]. While the focus in this study is on the amplifier errors itself, a more general approach studies the contribution of current amplifier errors in positioning systems by including the entire mechatronic control loop in the analysis [9], [10]. By doing so, also the effect of the position control dynamics and the mechanical system on the resulting positioning uncertainty can be studied.

The authors recently proposed a highly integrated model-based control structure for a switched amplifier-driven nano-positioning system [11]. In a dynamic error budgeting analysis, the dominant error sources affecting the positioning uncertainty are analyzed. It is shown, that the positioning uncertainty can be vastly reduced in comparison to a traditional cascaded frequency domain control structure, by attenuating the prevailing current measurement noise with the state-observer in the control. While the positioning uncertainty analysis in the study is focusing on the dominant error sources, a comprehensive dynamic error budgeting analysis including all possible error sources is beneficial for a deeper understanding of the entire mechatronic system. A general error budgeting framework is of great importance for scaling the system to different sizes or to adapt for different applications, because the dominance of each error source can vary depending on the specific system and controller parameters.

The contribution of this paper is the comprehensive analysis of different error sources affecting the positioning uncertainty in a switched amplifier-driven precision positioning system with integrated state-control structure. Additionally, an internal quantization error feedback in the state-observer of the control is introduced for uncertainty reduction.

II. System Description

This section introduces the developed switched amplifier-driven precision positioning system together with its integrated state-control structure based on a mathematical system model. A more detailed description of the system and the model derivation can be found in [11].

A. 1-DoF Precision Positioning System

The developed precision positioning system together with a compact custom made switched current amplifier is shown in Fig. 1. It allows precise positioning of a mover in one degree of freedom (DoF) by a Lorentz force based voice-coil actuator (VCA). The mover is restricted in the non-actuated DoFs by an aluminium flexure structure which is connected to the base of the system. An interferometric measurement system (IDS3010, AttoCube Systems AG, Germany) allows

The financial support by the Austrian Federal Ministry of Labour and Economy, the National Foundation for Research, Technology and Development and the Christian Doppler Research Association, and Micro-Epsilon Atensor GmbH and MICRO-EPSILON-MESSTECHNIK GmbH & Co.K.G. is gratefully acknowledged. Authors are with the Christian Doppler Laboratory for Precision Measurements in Motion, Automation and Control Institute, TU Wien. Corresponding author: pechgraber@acin.tuwin.ac.at

Pre-Print version of the article: D. Pechgraber, E. Csencsics, and G. Schitter, "Reducing the uncertainty in a switched amplifier-driven positioning system to the sub-nanometer level," *2024 IEEE/ASME International Conference on Advanced Intelligent Mechatronics (AIM)*, 2024. DOI: 10.1109/AIM55361.2024.10637163

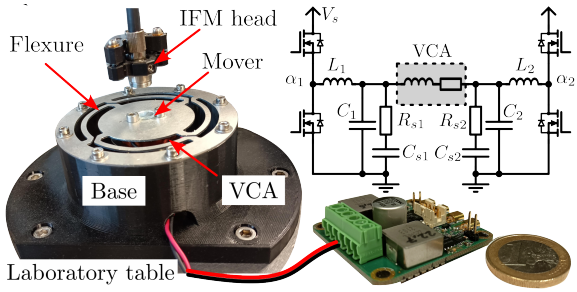

Fig. 1. Switched amplifier driven 1-DoF precision positioning system actuated by Lorentz-force based voice-coil actuator (VCA) [11].

measurements of the mover position in the sub-nm range. For the prototype the mover mass is kept as low as possible to enable high accelerations. Additionally, lighter masses are inherently more responsive to disturbance forces, which makes the system well suited for evaluating the presented error budgeting analysis and for showcasing the achievable precision with the switched current amplifier.

The amplifier consists of a MOSFET full-bridge structure with the VCA acting as the load in between two half-bridges, which allows driving the VCA in positive and negative direction with a single power supply V_s. The MOSFETs are PWM-modulated and switched according to the respective duty-cycles α_1 and α_2. Symmetric LC output filters on either side reduce the current ripple and unwanted EMI effects. To damp the resonance peak of the filter, additional snubber circuits (R_s, C_s) are added.

B. Mathematical Modeling

The goal is to have a mathematical model which incorporates the mechanical and electrical dynamics of the system from Fig. 1. For a generalized duty-cycle input α with $\alpha_1 = \alpha$, and $\alpha_2 = 1 - \alpha$ and under the assumption of symmetric component values on both sides ($L_1 = L_2$, $C_1 = C_2$, ...), the amplifier full-bridge circuit can be reduced to an equivalent state-space averaged circuit model according to Fig. 2 [11], [12]. With the supply voltage V_s and the

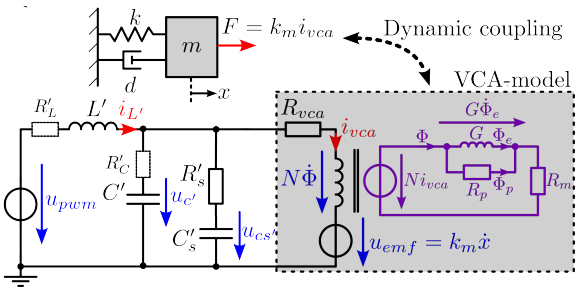

Fig. 2. Equivalent circuit model of switched amplifier for generalized duty-cycle input α and mechanical system model as mass-spring-damper system.

generalized duty-cycle α the input voltage of the model is expressed by $u_{pwm} = (2\alpha - 1)\,V_s$, with $\alpha \in [0, 1]$.

The mechanical system is modeled as a mass-spring-damper system, with the actuator force F acting on the mover mass m. For the VCA-model the inductance, copper resistance R_{vca} and the back-induced voltage into the coil u_{emf} are considered. Mostly a constant inductance is assumed, which is however not the case in reality due to eddy-current effects that lead to a reduction of inductance for higher frequencies [13]. This effect is included by splitting the VCA model in its electrical and magnetical domain, and by including a "magnetic inductance" G into the flux path [11], [14]. The coupling between these two domains is given by

$$Ni_{vca} = G\dot{\Phi}_e + R_m\Phi\,, \tag{1a}$$

$$u_{vca} = R_{vca}i_{vca} + N\dot{\Phi} + u_{emf}\,, \tag{1b}$$

$$\Phi_p = \frac{G\dot{\Phi}_e}{R_p}\,. \tag{1c}$$

Considering also the dynamical coupling to the mechanical domain, a linear state-space formulation of the entire system can be derived with the state-vector $\mathbf{x} = \left[\dot{x}\; x\; i_{L'}\; u_{c'}\; u_{cs'}\; \dot{\Phi}_e\; \Phi_e\right]^T$, the system input $u = u_{pwm}$, and the output $\mathbf{y} = \left[x\; i_{vca}\right]^T$ [11]:

$$\dot{\mathbf{x}} = \underbrace{\begin{bmatrix} \mathbf{A}_{11} & \mathbf{0} & \mathbf{A}_{13} \\ \mathbf{0} & \mathbf{A}_{22} & \mathbf{A}_{23} \\ \mathbf{A}_{31} & \mathbf{A}_{32} & \mathbf{A}_{33} \end{bmatrix}}_{\mathbf{A}} \mathbf{x} + \underbrace{\left[0\,0\,\tfrac{1}{L'}\,0\,0\,0\,0\right]^T}_{\mathbf{b}^T} u\,, \tag{2a}$$

$$\mathbf{y} = \underbrace{\begin{bmatrix} 0\,1\,0\,0\,0 & 0 & 0 \\ 0\,0\,0\,0\,0 & \frac{G(R_m+R_p)}{NR_p} & \frac{R_m}{N} \end{bmatrix}}_{\mathbf{C}} \mathbf{x}\,. \tag{2b}$$

The dynamic matrix $\mathbf{A}$ is partitioned into the mechanical part

$$\mathbf{A}_{11} = \begin{bmatrix} -\frac{d}{m} & -\frac{k}{m} \\ 1 & 0 \end{bmatrix}\,, \tag{3}$$

the electrical part

$$\mathbf{A}_{22} = \begin{bmatrix} \frac{(-R'_s-R'_L)R'_C-R'_sR'_L}{L'(R'_C+R'_s)} & \frac{-R'_s}{(R'_C+R'_s)L'} & \frac{-R'_C}{(R'_C+R'_s)L'} \\ \frac{R'_s}{C'(R'_C+R'_s)} & \frac{-1}{C'(R'_C+R'_s)} & \frac{1}{C'(R'_C+R'_s)} \\ \frac{R'_C}{C'_s(R'_C+R'_s)} & \frac{1}{C'_s(R'_C+R'_s)} & \frac{-1}{C'_s(R'_C+R'_s)} \end{bmatrix}\,, \tag{4}$$

and the magnetical part

$$\mathbf{A}_{33} = \begin{bmatrix} a_1 & a_2 \\ 1 & 0 \end{bmatrix}\,, \tag{5}$$

with

$$a_1 = \frac{-\left(\left(R_{vca}+R'_s\right)R'_C + R_{vca}R'_s\right)\left(R_m+R_p\right)}{N^2\left(R'_C+R'_s\right)} - \frac{R_p}{G}\,, \tag{6a}$$

$$a_2 = -\frac{R_m\left(\left(R_{vca}+R'_s\right)R'_C + R_{vca}R'_s\right)R_p}{G\,N^2\left(R'_C+R'_s\right)}\,. \tag{6b}$$

Pre-Print version of the article: D. Pechgraber, E. Csencsics, and G. Schitter, "Reducing the uncertainty in a switched amplifier-driven positioning system to the sub-nanometer level," *2024 IEEE/ASME International Conference on Advanced Intelligent Mechatronics (AIM)*, 2024. DOI: 10.1109/AIM55361.2024.10637163

The dynamic coupling between the 3 domains is given by the off-diagonal matrices

$$\mathbf{A}_{13} = \begin{bmatrix} \frac{Gk_m(R_m+R_p)}{R_pNm} & \frac{R_mk_m}{Nm} \\ 0 & 0 \end{bmatrix}, \quad \mathbf{A}_{31} = \begin{bmatrix} \frac{-R_pk_m}{NG} & 0 \\ 0 & 0 \end{bmatrix}, \tag{7a}$$

$$\mathbf{A}_{23} = \begin{bmatrix} \frac{GR'_sR'_C(R_m+R_p)}{NR_p\left(R'_C+R'_s\right)L'} & \frac{R'_CR'_sR_m}{N\left(R'_C+R'_s\right)L'} \\ \frac{-GR'_s(R_m+R_p)}{C'NR_p\left(R'_C+R'_s\right)} & \frac{-R'_sR_m}{C'N\left(R'_C+R'_s\right)} \\ \frac{-GR'_C(R_m+R_p)}{NR_p\left(R'_C+R'_s\right)C'_s} & \frac{-R'_CR_m}{C'_sN\left(R'_C+R'_s\right)} \end{bmatrix}, \tag{7b}$$

$$\mathbf{A}_{32} = \begin{bmatrix} \frac{R'_sR'_CR_p}{NG\left(R'_C+R'_s\right)} & \frac{R'_sR_p}{NG\left(R'_C+R'_s\right)} & \frac{R'_CR_p}{NG\left(R'_C+R'_s\right)} \\ 0 & 0 & 0 \end{bmatrix}. \tag{7c}$$

C. Integrated Control Structure

The integrated state-control structure is based on the derived state space-model (2) and is shown in Fig. 3. A

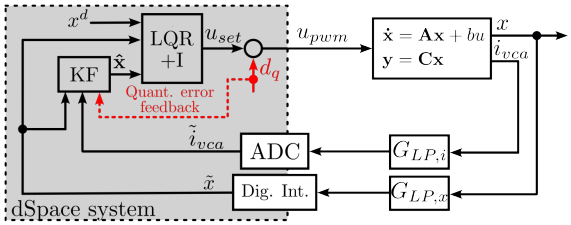

Fig. 3. Integrated state-control structure including a linear quadratic regulator (LQR) with additional integral state (I) and a kalman filter (KF) for estimation of the unmeasured states. The a-priori known PWM quantization error d_q is internally fed back to the KF in every cycle.

combination of an LQR with additional integral component (I) and a Kalman filter (KF) as state-observer are implemented in a rapid prototyping system (MicroLabBox, dSPACE GmbH, Germany). The measured actuator current i_{vca} is sampled by an analog-digital converter (ADC) and the mover position x is transferred via a digital interface. Due to the digital implementation of the control anti-aliasing filter ($G_{LP,i}$, $G_{LP,x}$) are added. As the goal is to track a desired reference position x^d, the LQR is formulated in the translated coordinates $\mathbf{z} = \mathbf{x} - \mathbf{x}_s$ and $u* = u - u_s$, with $\mathbf{x}_s$ and u_s being the steady-state state-vector and control input respectively, because the LQR usually stabilizes the zero state-vector. With the derived system model $\mathbf{x}_s$ and u_s are given by [11]

$$\mathbf{x}_s = \underbrace{\begin{bmatrix} 0 & 1 & \frac{k}{k_m} & \frac{R_{vca}k}{k_m} & \frac{R_{vca}k}{k_m} & 0 & \frac{Nk}{R_mk_m} \end{bmatrix}^T}_{\mathbf{X}} x^d, \tag{8a}$$

$$u_s = \underbrace{k\frac{R_L + R_{vca}}{k_m}}_{U} x^d. \tag{8b}$$

For the control design the system model (2) is discretized with the sampling time $T_s = \frac{1}{f_s}$ and an integrator state z^I is included

$$\mathbf{z}^a = \begin{bmatrix} \mathbf{z} \\ z^I \end{bmatrix}, \; z^I_{k+1} = z^I_k + T_s\left(x^d_k - \tilde{x}_k\right), \tag{9}$$

forming the augmented discrete time system

$$\mathbf{z}^a_{k+1} = \mathbf{\Phi}^a\mathbf{z}^a_k + \mathbf{\Gamma}^a u_k, \tag{10a}$$

$$y_k = \mathbf{C}^a\mathbf{z}^a_k. \tag{10b}$$

The added state, which integrates the difference between desired position x^d and the position measurement $\tilde{x}$, assures zero steady-state error due to model uncertainties or slowly changing system parameters. Taking (9) into account, the augmented state-space matrices result in

$$\mathbf{\Phi}^a = \begin{bmatrix} \mathbf{\Phi} & \mathbf{0} \\ -\mathbf{C}_1 & 0 \end{bmatrix}, \; \mathbf{\Gamma}^a = \begin{bmatrix} \mathbf{\Gamma} \\ 0 \end{bmatrix}, \tag{11}$$

with $\mathbf{\Phi}$ and $\mathbf{\Gamma}$ denoting the discretized dynamic matrix and input vector of the system, and $\mathbf{C}_1$ being the first row of the matrix $\mathbf{C}$. This is, because for the integral part only the position $\tilde{x}$ is considered. For this augmented system a discrete LQR is designed for the state-weighting matrix $\mathbf{Q} \in \mathbb{R}^{8\times8}$ and control output weighting $R \in \mathbb{R}$ with the Matlab command *lqrd*. In a similar manner the KF is designed with the noise covariance matrices $\mathbf{Q}_n \in \mathbb{R}^{7\times7}$ and $\mathbf{R}_n \in \mathbb{R}^{2\times2}$ with the command *kalmd*. Given the state estimate $\hat{\mathbf{x}}_k$ of the KF the control output u_{set} is calculated by

$$u_{set,k} = \underbrace{\begin{bmatrix} \mathbf{K}_z & K_I \end{bmatrix}}_{\mathbf{K}} \begin{bmatrix} \hat{\mathbf{x}}_k - \mathbf{x}_s \\ z^I_k \end{bmatrix} + u_s. \tag{12}$$

with $\mathbf{K}$ being the LQR gain. It is important to point out, that for the control the difference between state-estimate $\hat{\mathbf{x}}$ and steady-state vector $\mathbf{x}_s$ is used, because the LQR control design is done in the translated coordinates $\mathbf{z}$, and that the steady-state control input u_s is added to the output of the LQR.

Usually the measurements ($\tilde{x}$, $\tilde{i}_{vca}$) and the control output u_{set} are directly used for the state-estimation in the KF. However, in some applications the quantization of measurement signals can not be neglected and has to be considered in the KF design [15]. In this case the output voltage of the controller is quantized, because only a finite timing resolution can be achieved with the digital control system and therefore only certain minimum voltage steps can be outputted with the switched amplifier. For the implemented direct PWM-modulation scheme (constant switching frequency with variable duty-cycle) this quantization voltage steps are defined by the supply voltage V_s, the PWM switching frequency f_s and the clock-frequency of the digital system f_{clk} according to

$$q_{pwm} = 2V_s\frac{f_{sw}}{f_{clk}}. \tag{13}$$

The factor 2 results from the fact, that the entire positive and negative supply range is covered with the full-bridge topology (see Fig. 1). As the variables in (13) are known, the quantization error $d_q = u_{pwm} - u_{set}$ can be calculated a-priori in each sampling step of the controller by

$$d_q = \left\{\frac{u_{set}}{q_{pwm}}\right\} q_{pwm} - u_{set}, \tag{14}$$

Pre-Print version of the article: D. Pechgraber, E. Csencsics, and G. Schitter, "Reducing the uncertainty in a switched amplifier-driven positioning system to the sub-nanometer level," *2024 IEEE/ASME International Conference on Advanced Intelligent Mechatronics (AIM)*, 2024. DOI: 10.1109/AIM55361.2024.10637163

TABLE I
SYSTEM AND CONTROL PARAMETERS

Parameter	Nominal value	Parameter	Nominal value
$L_1 = L_2$	22.5 µH	m	$47{\cdot}10^{-3}$ kg
$R_{L1} = R_{L2}$	70 mΩ	k	$4.1{\cdot}10^{3}$ N/m
$C_1 = C_2$	15 µF	d	8.79 N s/m
$R_{C1} = R_{C2}$	10 mΩ	V_s	16 V
$C_{s1} = C_{s2}$	21 µF	f_s	50 kHz
$R_{s1} = R_{s2}$	1.35 Ω	f_{sw}	50 kHz
R_{vca}	5.36 Ω	f_{clk}	100 MHz
G	$1.98{\cdot}10^{3}$ 1/Ω	f_c	100 kHz
N	243	$n_{sens,i}$	$6{\cdot}10^{-12}$ A²/Hz
R_p	$1{\cdot}10^{8}$ 1/H	$n_{sens,p}$	$2{\cdot}10^{-23}$ m²/Hz
R_m	$3.47{\cdot}10^{7}$ 1/H		
k_m	12.87 N/A		
$\mathbf{Q}$	$\mathbf{diag}\left(1{\cdot}10^{7}, 4{\cdot}10^{13}, 1, 1, 1, 1, 5{\cdot}10^{19}\right)$		
R	1		
$\mathbf{Q}_n$	$\mathbf{diag}\left(10^{6}, 2.5{\cdot}10^{9}, 1, 1, 1, 1, 1\right) \cdot 10^{-6}$		
$\mathbf{R}_n$	$\mathbf{diag}\left(1{\cdot}10^{-12}, 0.3\right)$		

with $\{\bullet\}$ denoting the rounding operator to the nearest integer value. For this reason it is proposed, to use the quantized voltage u_{pwm} for the state-estimation instead of the ideal control output u_{set}. With the KF estimation gain $\mathbf{L}$ the state-estimation equation follows with

$$\hat{\mathbf{x}}_{k+1} = \mathbf{\Phi}\hat{\mathbf{x}}_k + \mathbf{\Gamma}(u_{set} + d_q) + \mathbf{L}\left(y_k - \mathbf{C}\hat{\mathbf{x}}_k\right) . \tag{15}$$

In Table I the identified system parameters and chosen control parameters are summarized.

III. POSITION UNCERTAINTY ANALYSIS

To analyze the control systems positioning uncertainty, dynamic error budgeting is used, in which the propagation of different error sources through the control circuit is analyzed in the frequency domain [16], [17]. Therefore the frequency domain representation of the plant and the controller is required, which will be introduced in this section together with the error sources affecting the precision of the system.

A. Frequency domain representation

While the frequency domain representation of the plant can be directly calculated from its state-space representation (2) via

$$\begin{bmatrix} G_{xu}(s) \\ G_{iu}(s) \end{bmatrix} = \mathbf{C}\left(s\mathbf{I} - \mathbf{A}\right)^{-1}\mathbf{b} , \tag{16}$$

it is not as intuitive with the controller. The control circuit from Fig. 3 is thus redrawn as shown in Fig. 4. The

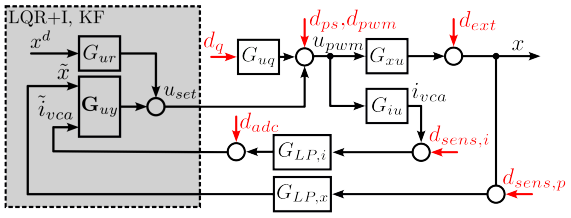

Fig. 4. Block diagram for dynamic error budgeting including all modeled error sources and frequency domain representation of system. The internal quantization error feedback is represented by the transfer function G_{uq}.

combination of KF and LQR+I control can be represented by the transfer function G_{ur} from the reference position x^d to the control output u_{set}, and the transfer matrix $\mathbf{G}_{uy} \in \mathbb{R}^{1\times 2}$ from the measurement to the control output. These transfer functions are derived by combining the z-transform of (8), (9), (12), and (15) and solving for u_{set}, resulting in [11]

$$\begin{aligned} u_{set} = &\underbrace{\left(1 - \mathbf{K}_z\mathbf{\Lambda}\mathbf{\Gamma}\right)^{-1}\left(\mathbf{K}_z\mathbf{\Lambda}\mathbf{L} - \frac{K_I}{z-1}\begin{bmatrix}1 & 0\end{bmatrix}\right)}_{\mathbf{G}_{uy} = \begin{bmatrix} G_{ux} \\ G_{ui}\end{bmatrix}}\underbrace{\begin{bmatrix}\tilde{x} \\ \tilde{i}_{vca}\end{bmatrix}}_{\mathbf{y}} \\ &+ \underbrace{\left(1 - \mathbf{K}_z\mathbf{\Lambda}\mathbf{\Gamma}\right)^{-1}\left(U + \frac{K_I}{z-1} - \mathbf{K}_z\mathbf{X}\right)}_{G_{ur}} x^d , \end{aligned} \tag{17}$$

with the matrix $\mathbf{\Lambda} = \left(z\mathbf{I} - \mathbf{\Phi} + \mathbf{LC}\right)^{-1}$. The internal quantization error feedback is represented by the transfer function G_{uq}, which is derived in a similar manner resulting in

$$G_{uq} = \left(1 - \mathbf{K}_z\mathbf{\Lambda}\mathbf{\Gamma}\right)^{-1} . \tag{18}$$

B. Error sources

The positioning uncertainty of the system is influenced by several error sources distributed across different locations, as depicted with the red arrows in Fig. 4. Certain error sources are of linear nature and can be accurately modeled as noise sources with well-defined power spectral densities (PSDs), such as the position measurement noise ($d_{sens,p}$), and current measurement noise ($d_{sens,i}$). These values can be determined by measurement or datasheet values. Considering that the position and current are sampled with the sample frequency f_s they are multiplied with some factor k_a to account for aliased noise components with frequencies greater than the Nyquist frequency $f_n = \frac{f_s}{2}$ of the control system. This value is calculated based on the cut-off frequency of the respective anti-aliasing low-pass filter ($G_{LP,i}$, $G_{LP,p}$) f_c and with its equivalent noise bandwidth $f_{enb} = \frac{\pi}{2} f_c$ [18]. It is assumed that up to this frequency f_{enb} the noise can pass the filter with unity gain and afterwards is perfectly suppressed. The additional aliasing factor is calculated by

$$k_a = \frac{f_{enb}}{f_n} = \frac{\pi}{2} f_c \frac{2}{f_s} = \pi \frac{f_c}{f_s} . \tag{19}$$

Another error source of linear nature are external disturbances (d_{ext}), which are dominated by vibrations of the environment, which are transmitted to the mover via the flexure and act as a disturbance force to the mover. These vibrations can vary over time, but still a worst-case PSD can be assumed for modeling the effect on the overall positioning precision. This is done by recording the position signal x with disabled controllers for several seconds and performing a Fast Fourier Transform (FFT) on the time-domain data. It has to be noted, that in this measurement also the position sensor noise ($d_{sens,p}$) is included, but this noise is sufficiently low to justify this assumption.

Pre-Print version of the article: D. Pechgraber, E. Csencsics, and G. Schitter, "Reducing the uncertainty in a switched amplifier-driven positioning system to the sub-nanometer level," *2024 IEEE/ASME International Conference on Advanced Intelligent Mechatronics (AIM)*, 2024. DOI: 10.1109/AIM55361.2024.10637163

Among the other category are the PWM-switching, and quantization errors of the system, which only can be approximated to a certain extent in the linear model. Additionally to the PWM-quantization error (d_q), which is already described in the previous section (refer to (13)), also the quantization of the analog-digital converter used for reading in the current measurement adds an additional error to the system (d_{adc}). The quantization errors are approximated by a white frequency distribution up to the nyquist frequency f_n of the system according to

$$PSD_q = \frac{q^2}{12 f_n}\,, \tag{20}$$

with the quantization step size q.

Of course also the PWM-switching itself contributes to the position errors (d_{pwm}). In general the output spectrum of a PWM-modulator is given by a carrier dependent spectrum, a signal dependent spectrum and the input signal itself [19]. Due to the fact, that it is hard to predict the output spectrum of the controller, and therefore the input signal of the PWM modulator, only the carrier dependent spectrum up to the 5th harmonic of the switching frequency is considered in this analysis. Furthermore it is assumed, that the control bandwidth is sufficiently low in comparison to the PWM-switching frequency f_{sw}, and therefore no inter-modulation occurs. The carrier dependent output spectral density, which is added to the signal itself, is given by [19]

$$d_{pwm}(f) = \sum_{k=0}^{\infty} \frac{2V_s}{\pi\,(2k+1)} \delta\left(f - (2k+1)\,2f_{sw}\right)\,. \tag{21}$$

The factor 2 at the switching frequency f_{sw} results from the used PWM-modulation scheme in the full-bridge circuit from Fig. 1 [11].

The power-supply noise of the amplifier circuit (Fig. 1) is modeled by adding d_{PS} on the output of the switched amplifier. As the VCA is the bridge-tied load between two half-bridges which are supplied by the same supply voltage V_s (refer to Fig. 1), the amount of noise on the VCA-voltage is dependent on the duty-cycle value. For $u_{pwm} = 0\,\mathrm{V}$, which corresponds to a duty-cycle $\alpha = 0.5$ both half-bridges are switched synchronously, which eliminates this noise from the VCA-voltage, whereas the worst-case is reached for $\alpha = 1$, in which one half-bridge is switched on permanently and all of the noise is added to the VCA-voltage. As usually a flexure guided positioning system is driven around its equilibrium position ($x = 0$) the evaluation is done for the case of $\alpha = 0.5$. In Table II the modeled error sources with their respective PSD calculation formula are summarized together with the simplifications made in the analysis.

C. Sensitivity Functions

In order to calculate the position error contribution of each error source, the sensitivity functions from each error source's locations to the position output has to be calculated. The procedure is similar for all error sources and is demonstrated in the following for the current measurement noise $d_{sens,i}$.

1) Set the input r and every error source except $d_{sens,i}$ to zero (superposition principle).
2) Calculate the plant transfer functions G_{xu} abd G_{iu} from (2) and the controller transfer matrix $\mathbf{G}_{uy}$ from (17).
3) Use the block-diagram (Fig. 4) and solve for $x(s)$ depending on $d_{sens,i}(s)$ in the Laplace domain.
4) The error sensitivity function is then calculated by $S_{sens,i}(s) = \frac{x(s)}{d_{sens,i}(s)}$.

The error sensitivity function for $d_{sens,i}$ is given by

$$S_{sens,i}(s) = \frac{G_{ui} G_{xu} G_{LP,i}}{1 - G_{ui} G_{iu} G_{LP,i} - G_{ux} G_{xu} G_{LP,x}}\,. \tag{22}$$

In Fig. 5 all sensitivity functions from each error source location (refer to Fig. 4) are shown for the the given system parameters from Table I. It is evident from the calculated

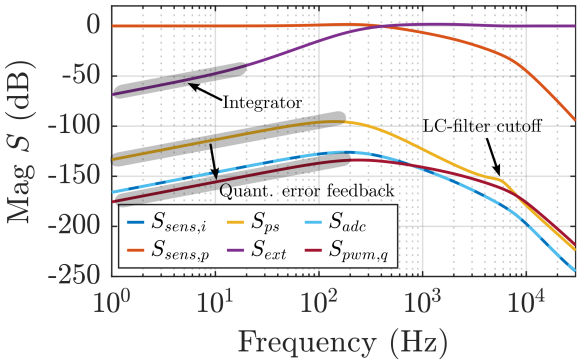

Fig. 5. Sensitivity functions from each error sources location to the position x. Due to the internal quantization error feedback the quantization error is reduced vastly in the lower frequency range (S_{ps} vs. $S_{pwm,q}$).

transfer functions, that beside the good attenuation of external disturbances at very low frequencies due to the integrator component in the control, the KF attenuates the current measurement noise quite well, which is the reason for the improved position precision as compared to a conventional frequency domain cascade controller [11]. Furthermore, the inclusion of the proposed internal quantization error feedback (refer to Fig. 3 and (15)) improves the susceptibility to PWM-quantization error in the lower frequency domain. This can be seen by comparing $S_{pwm,q}$ to the power-supply noise sensitivity function S_{ps}, because without internal quantization feedback, the quantization error enters the system at the location of d_{ps}.

IV. Evaluation

A. Simulation Model

To evaluate the modeled error sources, additionally to the experiments on the prototype system (Fig. 1) a time-domain simulation in Simulink (Matlab, MathWorks, CA, USA) is performed, including all the non-linearities that can only be approximated in the linear model, like the PWM-switching, the quantization or the discrete implementation of the control. The implementation details of each error source

Pre-Print version of the article: D. Pechgraber, E. Csencsics, and G. Schitter, "Reducing the uncertainty in a switched amplifier-driven positioning system to the sub-nanometer level," *2024 IEEE/ASME International Conference on Advanced Intelligent Mechatronics (AIM)*, 2024. DOI: 10.1109/AIM55361.2024.10637163

TABLE II
PSD CALCULATION OF ERROR SOURCES AND IMPLEMENTATION IN TIME-DOMAIN SIMULATION

Error source	Power spectral density for DEB	Simplification made	Implementation in simulation
$d_{sens,i}$	$n_{sens,i}k_{a,i}$	-	White noise source
$d_{sens,p}$	$n_{sens,p}k_{a,p}$	-	White noise source
d_{ps}	n_{ps}	Noise depends on α	White noise added in PWM-modulator supply
d_{ext}	n_{ext}	$n_{sens,p}$ included in measurement	Inject measured signal of ext. disturbances
d_{pwm}	$\sum_{k=0}^{5}\left[\frac{2V_s}{\pi(2k+1)}\delta\left(f-(2k+1)\,2f_{sw}\right)\right]$	Only carrier harmonics considered (1-5)	PWM-switching included
d_{adc}	$\frac{q_{adc}}{6f_s}$, $q_{adc}=\frac{FSR}{2^{bit}}=\frac{20\,\mathrm{V}}{2^{16}}$	White-noise assumption	Quantizer + zero-order hold
d_q	$\frac{q_{pwm}}{6f_{sw}}$, $q_{pwm}=2V_s\frac{f_{sw}}{f_{clk}}$	White-noise assumption	Quantizer before PWM-modulator

are listed in Table II. Each error source can be activated and deactivated in the model, to evaluate the effect of each error source on the position output separately, which is not possible experimentally. Therefore the time-domain signal of the simulation is used to calculate the frequency domain uncertainty spectrum with the FFT for several simulation runs with different activated error sources.

B. Evaluation of Dynamic Error Budget

With the PSD of the modeled error sources (Table II) and sensitivity functions, the resulting PSD on the position output x can be calculated for each error source by [20]

$$|PSD_{x,i}(f)| = |PSD_i(f)|\,|S_i(f)|^2\,, \tag{23}$$

with i referring to the respective error source and corresponding sensitivity function. If it is further assumed that the error sources are not correlated with each other, the total PSD of the position output is simply the sum over all parts.

In Fig. 6 the square-root of the cumulative PSD is plotted, representing the cumulative amplitude spectrum density (ASD), which can directly be related to the resulting uncertainty RMS-values. The solid lines represent the contribution of each modeled error source to the output uncertainty and the red dashed line represents the sum over all error sources. The time-domain simulations are marked with circles and it can be seen, that they match the theoretical analysis very well, which confirms the underlying modeling assumptions. However, for the PWM-switching the simplifications made lead to the first error component at the 1st switching harmonic at 100 kHz, whereas the signal dependent spectrum is neglected. This leads to the deviation in the graph of approximately a factor 2, but as the overall contribution to the position uncertainty is a few decimal powers below the other error sources this has no significant influence on the total result. Another divergence can be observed in the PWM-switching quantization error. The reason is, that for the underlying assumption of white-noise quantization error, the input signal of the quantizer has to be sufficiently higher than the quantization steps itself, which is not the case for this system. This leads to non-linear limit-cycling effects due to the integrator included in the control and to an overall worse error than predicted by the simple linear model [21]. This error is also dependent on the steady-state position value, as the necessary output voltage for holding this position is located at different relative positions inside an output voltage quantization step (refer to (13)). Despite the deviation, the theoretical assumption can be used as a guideline during system design, which however should be verified in time-domain simulation. It is to note that the power-supply noise is not visible in this graph because for the evaluated steady-state operation point theoretically the noise perfectly cancels out due to the PWM-modulation scheme of the current amplifier (refer to Section III-B).

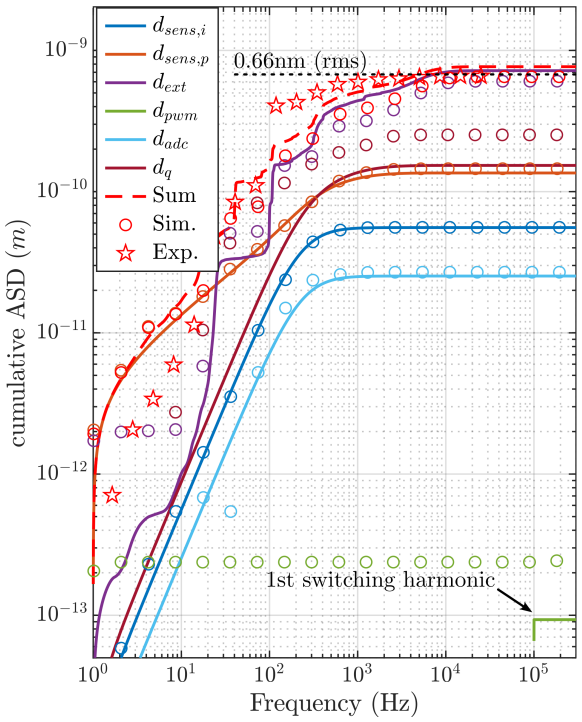

Fig. 6. Cumulative amplitude spectrum density (ASD) of position error contribution of each error source via dynamic error budgeting (solid lines, dashed line), together with results from time-domain simulation (circles) and experimental result (red stars).

On top of the theoretical curves the measurement from the experimental prototype setup is plotted with red stars, confirming the validity of the simulation and theoretical analysis, and showing an extraordinary low steady-state uncertainty of 0.66 nm (rms).

Pre-Print version of the article: D. Pechgraber, E. Csencsics, and G. Schitter, "Reducing the uncertainty in a switched amplifier-driven positioning system to the sub-nanometer level," *2024 IEEE/ASME International Conference on Advanced Intelligent Mechatronics (AIM)*, 2024. DOI: 10.1109/AIM55361.2024.10637163

C. Evaluation in the time-domain

To evaluate the dynamics of the control and performance of the proposed internal quantization error feedback, the response to several 5 nm steps on the reference input is shown in Fig. 7. The proposed integrated state-control scheme

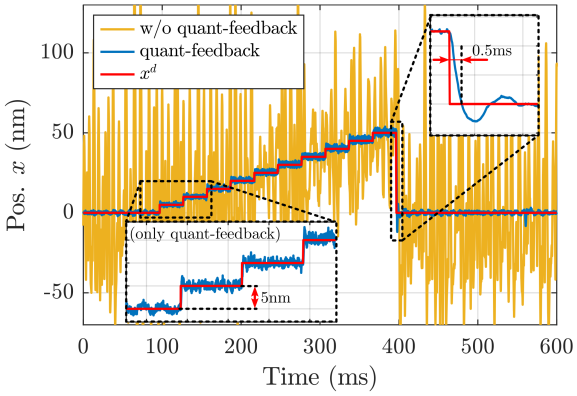

Fig. 7. Response to 5nm-steps on the reference input x^d. The integrated state-control scheme shows a rise-time of 0.5 ms. With the internal quantization error feedback the positioning uncertainty can be improved by a factor of 65 from 43 nm to 0.66 nm (rms).

shows fast reference position tracking with 0.5 ms rise-time in response to the negative 50 nm step. As predicted by the sensitivity function $S_{pwm,q}$ from Fig. 5, the internal quantization error feedback vastly improves the positioning uncertainty by a factor of 65 from 43 nm to 0.66 nm (rms). The achieved precision in the time-domain plot confirms the results from the dynamic error budget analysis in the frequency domain.

In summary, the effectiveness of the analytical dynamic error budget analysis for the estimation of the positioning uncertainty is successfully demonstrated in time-domain simulation and on an experimental prototype setup. Additionally it is shown, that by introducing an internal quantization error feedback in the state-estimator of the control, the susceptibility to PWM-quantization errors can be reduced, enabling sub-nanometer positioning uncertainty.

V. Conclusion

This paper presents a comprehensive position uncertainty analysis for a switched amplifier-based high-precision positioning system with integrated full-state control structure. The theoretical results from the dynamic error budgeting analysis are validated by time-domain simulations and by experiments on an experimental prototype system. With the proposed control scheme extremely fast reference position tracking with a rise-time of 0.5 ms on a step-response can be shown. Additionally the integration of an internal quantization error feedback in the state-observer improves the positioning uncertainty by a factor of 65 to 0.66 nm (rms), enabling positioning resolutions in the sub-nanometer range.

References

[1] H. Butler, "Position control in lithographic equipment [applications of control]," *IEEE Control Systems*, vol. 31, no. 5, pp. 28–47, 2011.
[2] G. Schitter, K. J. Astrom, B. E. DeMartini, P. J. Thurner, K. L. Turner, and P. K. Hansma, "Design and modeling of a high-speed AFM-scanner," *IEEE Transactions on Control Systems Technology*, vol. 15, no. 5, pp. 906–915, 2007.
[3] L. Jonušauskas, D. Gailevičius, S. Rekštytė, T. Baldacchini, S. Juodkazis, and M. Malinauskas, "Mesoscale laser 3d printing," *Optics Express*, vol. 27, no. 11, p. 15205, 2019.
[4] S. Ito, J. Steininger, and G. Schitter, "Low-stiffness dual stage actuator for long rage positioning with nanometer resolution," *Mechatronics*, vol. 29, pp. 46–56, 2015.
[5] S. Ito, S. Pirker, and G. Schitter, "Integrating PWM amplifier with the design of mechatronic systems for energy-efficient precision motion," *IEEJ Journal of Industry Applications*, vol. 10, no. 2, pp. 134–141, 2021.
[6] P. Sriyotha, K. Nakamoto, M. Sugai, and K. Yamazaki, "Development of 5-axis linear motor driven super-precision machine," *CIRP Annals*, vol. 55, no. 1, pp. 381–384, 2006.
[7] T. Riel, R. Saathof, A. Katalenic, and G. Schitter, "Noise analysis and improvement of a permanent magnet synchronous motor by dynamic error budgeting," *IFAC-PapersOnLine*, vol. 49, no. 21, pp. 339–346, 2016.
[8] F. A. Qureshi, V. Spinu, K. Wijnands, and M. Lazar, "A real-time control system architecture for industrial power amplifiers," in *2013 American Control Conference*, IEEE, 2013.
[9] S. J. Settels, J. van Duivenbode, and J. L. Duarte, "Impact of amplifier errors on position loop accuracy of high-precision moving stages," in *2017 19th European Conference on Power Electronics and Applications (EPE'17 ECCE Europe)*, IEEE, 2017.
[10] M. Hajiheidari, D. Xu, J. van Duivenbode, B. Vermulst, and M. Lazar, "Analysis of power amplifier contribution to the precision of motion systems," in *2022 IEEE 17th International Conference on Advanced Motion Control (AMC)*, IEEE, 2022.
[11] D. Pechgraber, E. Csencsics, J. Wiesböck, and G. Schitter, "Switched amplifer driven positioning system with single nanometer precision," *IEEE Trans. on Ind. Electron.*, 2023. (Under Review).
[12] N. Mohan, T. M. Undeland, and W. P. Robbins, *Power electronics: converters, applications, and design*. John wiley & sons, 2003.
[13] F. Cigarini, S. Ito, S. Troppmair, and G. Schitter, "Comparative finite element analysis of a voice coil actuator and a hybrid reluctance actuator," *IEEJ Journal of Industry Applications*, vol. 8, no. 2, pp. 192–199, 2019.
[14] A. Brown, J. Ross, and K. Nichols, "Time-domain simulation of mixed nonlinear magnetic and electronic systems," *IEEE Transactions on Magnetics*, vol. 37, no. 1, pp. 522–532, 2001.
[15] J. Xu, J.-x. Li, and S. Xu, "Quantized innovations kalman filter: stability and modificationwith scaling quantization," *Journal of Zhejiang University SCIENCE C*, vol. 13, no. 2, pp. 118–130, 2012.
[16] L. Jabben and J. Van Eijk, "Performance analysis and design of mechatronic systems," *Mikroniek*, vol. 51, no. 2, pp. 5–12, 2011.
[17] T. Riel, R. Saathof, A. Katalenic, S. Ito, and G. Schitter, "Noise analysis and efficiency improvement of a pulse-width modulated permanent magnet synchronous motor by dynamic error budgeting," *Mechatronics*, vol. 50, pp. 225–233, 2018.
[18] Texas Instruments, "Noise analysis in operational amplifier circuits," 2007.
[19] Z. Song and D. V. Sarwate, "The frequency spectrum of pulse width modulated signals," *Signal Processing*, vol. 83, no. 10, pp. 2227–2258, 2003.
[20] W. A. Gardner, *Introduction to random processes*. McGraw-Hill, 1989.
[21] A. Peterchev and S. Sanders, "Quantization resolution and limit cycling in digitally controlled PWM converters," *IEEE Transactions on Power Electronics*, vol. 18, no. 1, pp. 301–308, 2003.

Pre-Print version of the article: D. Pechgraber, E. Csencsics, and G. Schitter, "Reducing the uncertainty in a switched amplifier-driven positioning system to the sub-nanometer level," *2024 IEEE/ASME International Conference on Advanced Intelligent Mechatronics (AIM)*, 2024. DOI: 10.1109/AIM55361.2024.10637163